Cold Gas Spray Inner Diameter Coatings and Their Properties

Joachim Meeß[1] · Manuel Anasenzl[1] · Ralf Ossenbrink[2] · Vesselin Michailov[2] ·
Reeti Singh[3] · Jan Kondas[3]

Abstract Due to recent developments, cold gas spraying technology can now be used to create inner diameter coatings for cylinder inner diameters > 70 mm. The present investigations focus on the process optimization and the specific properties of cold gas spray inner diameter coatings created with three different alloy steel powder variants. The cold gas spray coating properties were compared with the corresponding properties of coatings created with twin wire arc technology. The particle velocities and deposition efficiencies were measured with the aim of optimizing the process parameters. The most suitable process parameters were used to analyze the microstructure of the deposited coating in terms of porosity and interface quality. Furthermore, the hardness and adhesion strength properties of the coatings were measured. In addition, the different liners were honed, and the achievable surface roughness of each was determined. Finally, wear resistance was evaluated using ball-on-disk testing. The results reveal that with the maximum process parameters, the cold gas spray coating properties are comparable to the twin wire arc coating properties. Further investigations are necessary to determine whether cold gas spraying is a feasible alternative to the current series production process for cylinder surface coatings.

✉ Joachim Meeß
  joachim.meess@bmw.de

  Manuel Anasenzl
  manuel.j.anasenzl@bmw.de

  Ralf Ossenbrink
  ralf.ossenbrink@b-tu.de

  Vesselin Michailov
  fg-fuegetechnik@b-tu.de

  Reeti Singh
  rs@impact-innovations.com

  Jan Kondas
  jk@impact-innovations.com

[1] BMW AG, Ohmstr. 2, 84030 Landshut, Germany

[2] Department Joining and Welding Technology, BTU Cottbus–
   Senftenberg, Konrad-Wachsmann-Allee 17, 03046 Cottbus,
   Germany

[3] Impact Innovations GmbH, Bürgermeister-Steinberger-Ring
   1, 84431 Rattenkirchen, Germany

Introduction

In the automotive industry, the requirements for emission limit values continue to rise. To achieve these goals, friction in combustion engines must be further reduced. The piston group consisting of the piston, piston ring and cylinder running surface is responsible for 30-48% of the friction in the engine. In the past, cylinder crankcases were made of gray cast iron. To reduce weight, crankcases were eventually made of an aluminum-silicon cast alloy, in which the gray cast iron liners were pressed. Due to some advantages in material properties, the gray cast iron liners were eventually replaced by thermal spray coatings. These advantages include higher wear resistance, higher component lifetime, reduced component costs and reduced weight (Ref 1-6).

Currently, various thermal spray processes exist to coat cylinder surfaces: twin wire arc (TWA), plasma transferred wire arc (PTWA), atmospheric plasma spraying (APS) and high-velocity oxy-fuel (HVOF) processes (Ref 7, 8). A

distinction is made between wire-based and powder-based processes. In wire-based processes, the choice of materials is limited since the wires must be electrically conductive and ductile (Ref 9). In powder-based processes, the raw material can vary more widely in terms of its chemical composition and therefore more easily influence the properties of the coating (Ref 10). Most thermal spray processes require the surface to be roughened prior to coating using various preparation methods known as activation. The surface can be activated using high-pressure water jets, grit blasting, laser texturing or mechanical processing. Deploying these surface preparations, an adhesion strength in the range of 40-58 MPa is achievable between the surface and coating for aluminum crankcases (Ref 9-12).

One of the most innovative thermal spraying methods is cold gas spraying (CGS). The cold spray process was developed in the mid-1980s at the Institute of Theoretical and Applied Mechanics of the Russian Academy of Science in Novosibirsk (Ref 13). CGS is a solid-state process in which powder particles are coated onto a substrate well below their melting point (Ref 14). With a standard CGS device, powder particles (5-50 μm) are accelerated to a high velocity of 300-1200 m/s by a supersonic gas jet in the divergent section of a de Laval nozzle. In doing so, the surface does not have to be specially roughened, as with other thermal spray technologies, to ensure that the coating adheres to the substrate (Ref 15). The achievable adhesion strength strongly depends on the applied process parameters, such as the gas temperature, gas pressure, powder feed rate and coating speed. For instance, using a 316L powder on an aluminum substrate can lead to high adhesion strengths of more than 60 MPa (Ref 16-18).

In recent years, CGS has also been expanded to a variety of application areas in industry (Ref 19-22). For inner diameter coating with CGS, a 90° angled head with a shorter nozzle is required. Due to recent developments, this technology can also be used for coating in cylinder blocks with a minimum diameter of 70 mm. The nozzle for the inner diameter coating is more than 50% shorter than a nozzle for the external diameter coating ("straight nozzle" with a length > 110 mm) (Ref 23, 24). Therefore, the shorter nozzle reduces the particle velocity and consequently attains different coating properties (e.g., deposition efficiency (DE)). In contrast, the cold spray equipment used for external coating (longer nozzle) can achieve a DE of 89% with 316L at 40 bar and 800 °C (Ref 25).

The aim of this study was to determine suitable process parameters for the inner diameter coating of three different alloy steel powders with different chemical compositions, particle sizes and morphologies using the CGS process with an adapted CGS system, as well as to analyze and evaluate the characteristics of the deposited coatings. The impacts of various process parameters were investigated in

terms of particle velocity and DE. Furthermore, the coatings were characterized by their porosity, hardness and adhesion strength properties. Finally, the coated liners were honed (postprocessing), and the wear resistance was measured. A comparison of the process properties between the CGS equipment for external coatings (longer nozzle) and the CGS equipment for inner diameter coatings (90° angled head with short nozzle) as well as a comparison of the coating properties between the CGS coating and the established cylinder surface coating (TWA) are presented.

Experimental Procedure

Cold Spray Experimental Setup

The experiments were carried out with an adapted prototype CGS system–inner diameter coating gun (Impact Innovations GmbH; Rattenkirchen, Germany). The inner diameter coating gun has a 90° angled head with a short nozzle for liners with an inside diameter of more than 70 mm. The rotating inner diameter coating gun turns on its own axis, unlike the standard CGS equipment. In this study, nitrogen was used as the process gas. Figure. 1 shows a schematic display of the experimental setup with the angle head inserted into the liner during CGS.

In the present research, three different iron-based powder types (316L, M3/2 and E) with different particle size
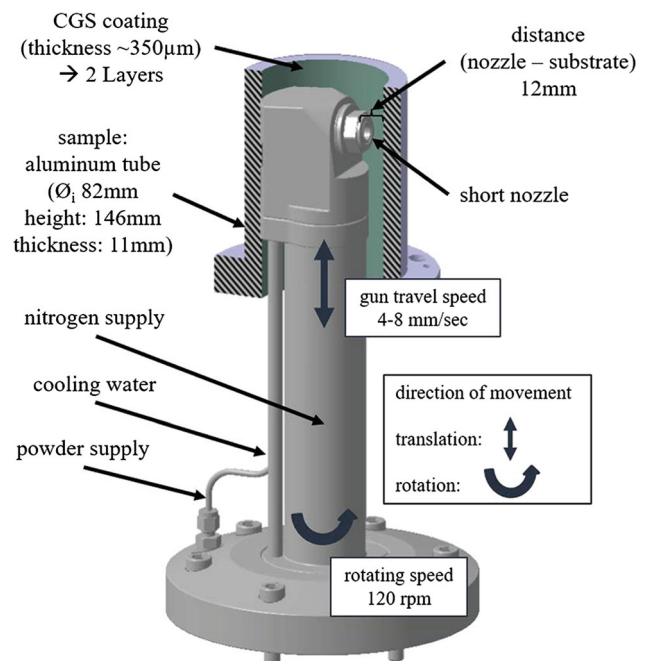
Fig. 1 Schematic display of the experimental setup with the angle head inserted into the liner during CGS with a rotating inner diameter coating gun

distributions (316L: 5-25; M3/2: − 45; and E: − 20 μm) were used. 316L is a commercially available stainless steel powder from Sandvik Osprey, Ltd. (Neath, Great Britain), which is atomized using nitrogen gas. M3/2 is a water-atomized tool steel powder with some carbides (MC and M_6C) from Höganäs AB (Höganäs, Sweden). Powder E is also a water-atomized powder and was supplied by Höganäs AB for this study. In addition, scanning electron microscopy (SEM) images were taken with a SEM Zeiss EVO 60 XVP to evaluate the morphology of the powder particles. The chemical analyses of the powder particles and the coating were carried out with energy-dispersive x-ray spectroscopy (EDX). EDX was carried out on the powder within five measuring ranges, whereas EDX was carried out on the coating within a measuring range with dimensions of 100×65 μm. The particle size distributions of all three powder variants were measured using a Cam-sizer X2.

Instead of crankcases, aluminum cylinder liners (AlSi7MgCu0.5) were utilized to simplify handling and reduce costs. In the following investigations, aluminum liners were machined to an inner diameter of 82.38 ± 0.01 mm, coated, and then analyzed.

Preliminary tests were carried out for screening purposes. The following parameters were modified: gas pressure (50-60 bar), gas temperature (900-1000 °C) and powder feed rate volume (8.91-50.49 cm^3/min). The preliminary tests were performed to obtain velocity measurements and DE measurements. From these preliminary tests, the parameter set with the best results was used for the experiments on the aluminum liners.

Sample Characterization

The DE was determined by measuring the weight of the substrate before and after coating; specifically, calculating the difference (Δm_s) to relate the delta to the mass of feed powder (m_p) during the coating process.

$$DE = \frac{\Delta m_s}{m_p} \qquad \text{(Eq 1)}$$
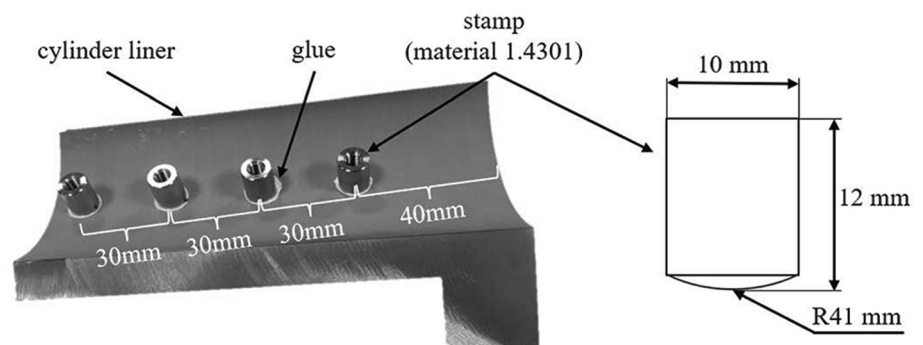
The particle velocity measurements were taken with a cold spray meter from Tecnar Automation Ltée (Saint-Bruno-de-Montarville, Canada). In this research, the distance from the measuring point to the nozzle was 5 mm. To determine the influence of the process parameters on the particle velocity, the gas pressure varied from 50 to 60 bar, and the powder feed rate varied from 8.91 to 50.49 cm^3/min.

Cross sections were taken to measure the coating porosity and the hardness of the coating. These cross sections were made by cutting the cylinder liners at the mid-section into small slices with a diamond blade. The samples were cold embedded and sequentially ground using silicon carbide grinding paper. Then, the cross sections were treated with grit paper and polishing pastes to reach to a surface quality of up to 1 μm. With these samples, micrographs were acquired by a light optical microscope Zeiss Axio Imager M2m. The Imagic IMS Image Processing V18Q4 software calculated the porosity of the coating by determining gray contrasts. The gray value thresholds were set manually in a defined test area of 1 mm^2. In this study, the threshold for powders 316L and E was set between 0 and 140, whereas the threshold for powder M3/2 was fixed between 0 and 60.

The coating hardness was measured by using a hardness tester from Qness Q10A+ in accordance with DIN EN ISO 6507 and measured with HV0.025. All measuring points were centralized in the middle between the substrate surface and the coating surface. .

The adhesion strength of the various coatings was measured with the "PosiTest AT-A" from DeFelsko. To achieve this, dome-shaped stamps (dome radius of 41 mm) were glued to the coated cylinder liner surface with an FM 1000 adhesive film from HTK Hamburg. Removal measurements were conducted after a curing time of one hour at 175 °C in the oven. The electronically controlled hydraulic pump automatically ensured an even and continuous release pressure of the dome-shaped stamps with a pull-off speed of 1.5 MPa/s. Figure. 2 shows the prepared coated cylinder surface for adhesion tests. This method is a

Fig. 2 Coated cylinder surface prepared for adhesion testing, and a schematic representation of the stamp

nonstandard test but was used to measure adhesion strength directly on the cylinder surface. The difference from the standard test (ASTM C633) is that in this test, the stamps are dome-shaped and not flat.

In addition, coated aluminum cylinder liners were diamond machined on a honing machine from Gehring Technologies GmbH (Ostfildern, Germany). Postprocessing consisted of three sequence steps: roughing, semifinishing and finishing.

Finally, the wear resistance of a CGS coating was measured using a ball-on-disk test. With the intention of generating flat and straight specimens for this experiment, which are required for the ball-on-disk test, a hexagon was machined into aluminum liners (see Fig. 3). The spray angle of the wear samples varied between 90 and 71° (21% maximum deviation), and the spray distance varied between 12 and 14 mm (17% maximum deviation). Flat samples (sample: 28 × 28 × 4 mm) were then cut out of the hexagonal liners. In this study, a steel ball (100Cr6)

served as the test body, applying a force of 10 N onto the wear-resistant specimen. Furthermore, the wear path on the sample was determined to be 3000 m with a test speed of 0.1 m/s. Figure 4 shows the experimental setup of the ball-on-disk test.

Results and Discussion

Powder Characterization

Figure 5 shows SEM images of all the powder variants used in this work: 316L (Fig. 5a), M3/2 (Fig. 5b) and E (Fig. 5c). 316L is almost spherical with some satellites surrounding the powder particles, M3/2 is elongated, whereas powder E has a morphology between those of 316L and M3/2. The shape of the particles is influenced by the manufacturing process (Ref 26). 316L is gas-atomized and therefore is expected to have spherical particles. Powders M3/2 and E are water-atomized and therefore have irregular particle shapes. Furthermore, carbides can be seen in powder M3/2 (MC and M6C), which offers a high level of wear resistance (Ref 27, 28).

Table 1 shows the particle size distributions of all three powder variants, which were measured using dry measurements on a Camsizer X2. The particle size distribution was specified in relation to the particle volume. The particle size distribution (d10-d90) was lowest for powder E with a range of 12.2 μm, followed by powder 316L with a range of 19.14 μm and lastly powder M3/2 with a range of 22.33 μm. For this reason, powder E agglomerated due to the fine particle size (the d90 value of powder 316L was 43% higher than the d90 of powder E), whereas powders M3/2 and 316L did not. Powders with very fine particles tend to form agglomerates, which can affect the CGS
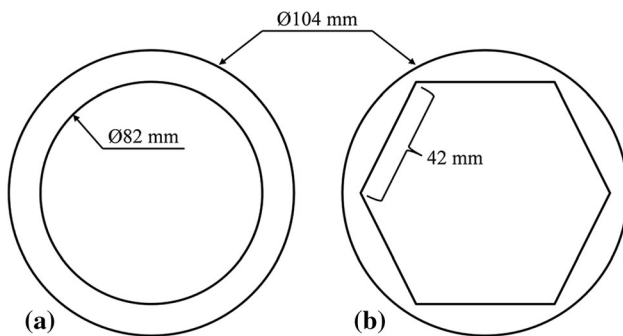
Fig. 3 Schematic representation of the liners: (a) internal contour: round with inner diameter 82 mm (b) internal contour: hexagon for wear-resistant samples
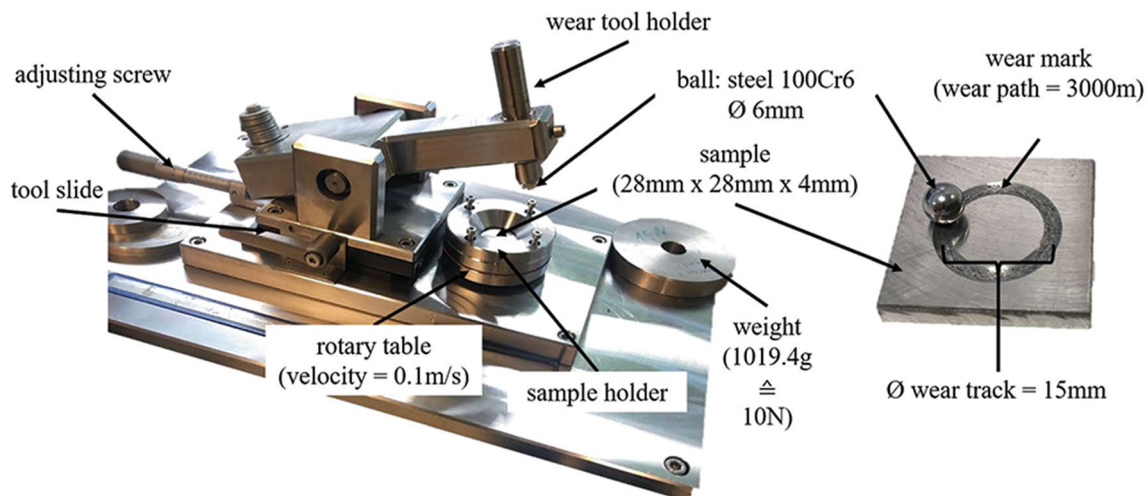
Fig. 4 Experimental setup of the ball-on-disk test
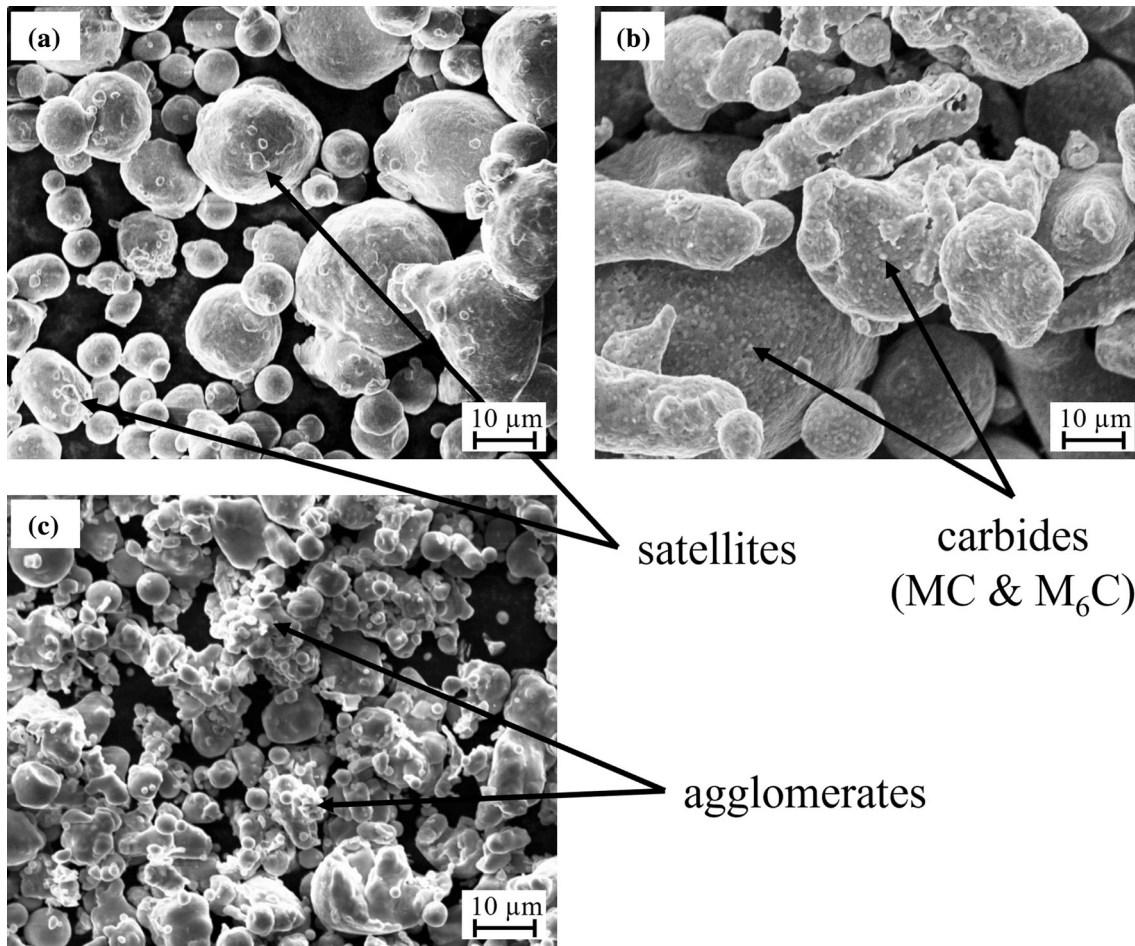
Fig. 5 SEM images of the powder used in the experiments: (a) 316L; (b) M3/2; (c) E

Table 1 Particle Size d10, d50 and d90

	316L	M3/2	E
d10 (μm)	8.09	17.49	6.97
d50 (μm)	14.79	28.72	12.42
d90 (μm)	27.23	39.82	19.07

process (Ref 29). Both the particle size and the morphology have a major influence on the coating process and coating properties (Ref 26).

Particle Velocity Measurement

Particle velocity measurements were taken to study the velocities of the different powder particles at different parameter settings. The gas pressure (50, 60 bar) and feed rate (8.91, 50.49 cm³/min) of each powder were varied. The temperature was set to a maximum of 1000 °C. Figure 6 shows that the average velocities of the 316L and M3/2 powders significantly decreased from 637 to 554 m/s and
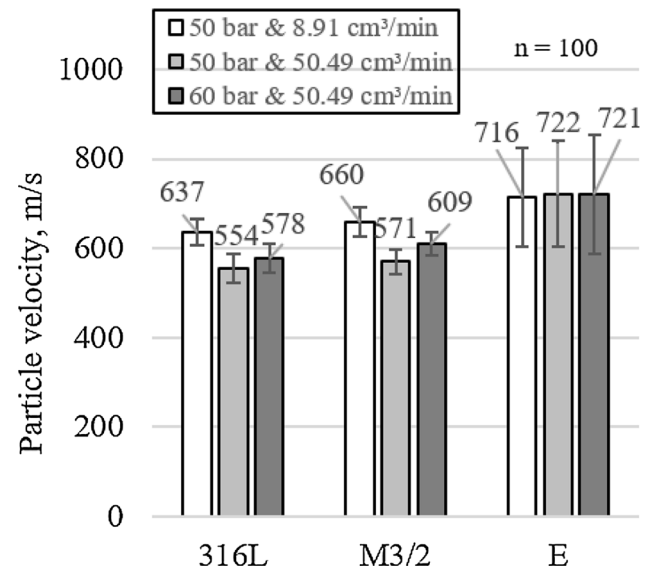
Fig. 6 Particle velocity at different gas pressures and feed rates. Powder variants used: 316L, M3/2 and E. Number of measurements = n. Error bars represent the standard deviation (1 sigma)

660 to 571 m/s, respectively, with increasing powder feed rate, which was modified from 8.91 to 50.49 cm³/min. An additional experimental setup was carried out with a fixed feed rate of 50.49 cm³/min and gas pressures set either to 50 or 60 bar. In this comparison, the average particle velocity increased slightly for the 316L and M3/2 powders at higher gas pressure levels (see Fig. 6). For powder E, no significant changes in the particle velocity were recognized, although the standard deviation was greater. Regarding this experimental outcome, the formed agglomerations of powder E are likely to influence the measurements and result in the observed greater standard deviations. Therefore, the speed measurement results of powder E must be interpreted with caution.

Throughout all the parameter set tests, the particle velocity of M3/2 was higher than that of 316L, although the particle size differed ($d90_{M3/2} > d90_{316L}$). In general, using CGS technology, particle velocities depend on the process parameters, powder particle size and powder morphology. Nonspherical particles can accelerate better than spherical particles at the same gas pressure and gas temperature. This could be one reason why in this study, the particle velocities of M3/2 were higher than those of 316L, which is in accordance with prior research (Ref 30-32). Powder E also has a nonspherical morphology, in addition to having the smallest particle size ($d90 = 19.07$ μm) of all the powders used. For this reason, the velocities peaked when utilizing powder E (due to its small particle size and irregular morphology).

It is known from the literature that with a similar cold spray device (CGS gun for inner diameter coating) and comparable process parameters (temperature of 900 °C, pressure of 50 bar, and powder feed rate of 4 kg/h), powder 316L can achieve particle velocities of approximately 700 m/s (Ref 23). Further investigations have also shown that the particle velocity increases with increasing gas pressure and gas temperature (Ref 23-25). Even for inner diameter coatings created with a shortened nozzle, the particle velocity increases with increasing process parameters.

Deposition Efficiency and Feed Rate

A high DE of the powder during CGS is important for cost-effective series production. DE measurements were taken in two sets at a designated gas pressure of 60 bar. In the first set, the powder feed rate was fixed to 8.91 cm³/min, whereas the gas temperature was varied from 900 to 1000 °C. The second set of DE measurements was conducted with a constant gas temperature of 1000 °C and a powder feed rate of either 8.91 or 50.49 cm³/min.

Figure. 7 illustrates the maximum DE for the inner diameter coating for all powders, which was, for example,
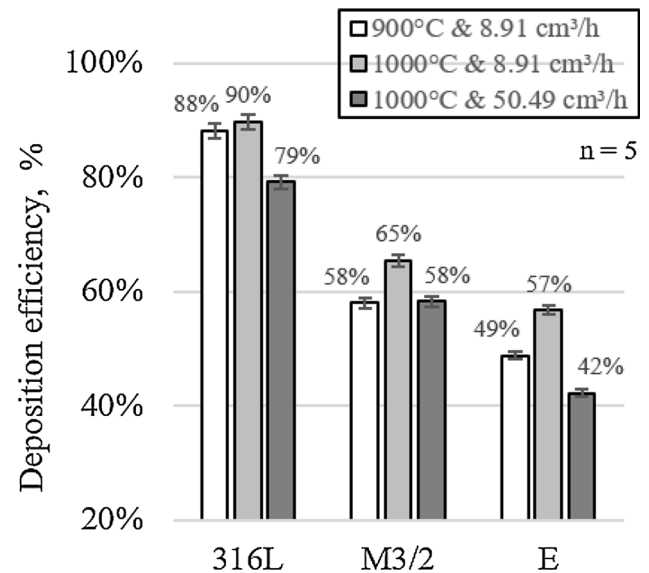
Fig. 7 DE at different gas temperatures and feed rates. Powder variants used: 316L, M3/2 and E. Number of measurements = n. Error bars represent the standard deviation (1 sigma)

90% for powder 316L when using optimal experimental conditions. In contrast, the DE maximum of powder M3/2 was 65%, while that of powder E peaked at 57%. However, the DE of all powders slightly increased with increasing gas temperature. In general, higher gas temperatures provide higher particle velocities, which then cause more particles to exceed the critical velocity, at which point deposition occurs (Ref 16). The related literature also suggests that high temperatures make the particles softer and therefore more likely to deposit (Ref 33, 34).

Furthermore, when increasing the powder feed rate from 8.91 to 50.49 cm³/min at 1000 °C, the DE considerably dropped (11 for powder 316L, 7 for powder M3/2 and 15% for powder E). One of the reasons for this could be that the 5.7 times higher feed rate of powder particles was accelerated with the same gas energy (gas pressure and gas temperature), resulting in reduced particle velocities and therefore decreased DEs. Likewise, the literature suggests that the particle speed decreases with increasing powder feed rate, causing the DE to deteriorate (Ref 23).

In comparison to the deposition properties defined here, longer CGS nozzles for external coatings have a DE of approximately 90%, which is already achieved at 800 °C and 40 bar (Ref 25).

It is clear that powder E, with the highest particle velocity and the lowest powder hardness, has the lowest DE. One reason for the low DE could be the agglomerates in the powder. The DE depends on the characteristics of the feedstock material, such as the material hardness, morphology and chemical composition of the powder (Ref 26-36). Since three alloy steel powders with different particle

sizes, morphologies, chemical compositions and manufacturing processes were used in this study, further investigations with fewer powder variables are needed to investigate the impact factors of the DE.

Because preliminary investigations have shown maximum process parameters to be suited for maximum outcome, the main studies for coating the liners adopted a maximum powder feed rate of 50.49 cm^3/min, a gas temperature of 1000 °C and a gas pressure of 60 bar. Following this process, the CGS coating was applied in two layers to a thickness of approximately 350 μm. To accomplish this, the robot kinematics (4-8 mm/s) had to be adjusted for the different powders due to the different DEs.

Microstructure

Table 2 shows the chemical composition of the different powders and the corresponding CGS coatings, which were determined by EDX analyses. For all three variants, the oxygen content within the coating structure increases compared to the oxygen level of the powder. This is due to oxidation during the coating process. The higher the temperature of the coating is, the higher the probability of oxidation (Ref 37, 38). The 316L coating has an oxygen content 225% greater than the corresponding powder, while the M3/2 and E coatings have oxygen contents 333 and 725% greater, respectively. Since the DE is lowest for powder E, the robot speed during coating is also lower, and the temperature in the coating is therefore the highest. No other changes in the chemical composition of the powder were observed during the CGS coating process.

Figure 8 shows the microscopic cross sections of the samples, which were obtained from the CGS coatings with the three powders: (a) 316L, (b) M3/2 and (c) E. The image shows that the brightest intensity was found in the aluminum substrate, while the dark gray component corresponds to the CGS coating. The black inclusions represent pores within the coating. In all cross sections, the interface between the coatings and the substrates was clear and continuous.

To analyze the quality of the coating, the porosity proportion was evaluated. Figure 9 highlights that the 316L coating had the highest porosity at 7.9%, whereas the coatings of powders M3/2 and E had significantly lower porosities (3.5 and 3.2%, respectively). This result was due to the lower particle velocity of powder 316L (see Fig. 6). During coating, the resulting porosity properties, especially the volume fraction and pore size, are determined by the temperature, pressure, particle size and particle velocity conditions (Ref 39). Powder morphology is also a key factor, which affects the attainable particle velocities (Ref 39, 40). These experiments indicate that the achievable porosities in CGS coatings on liners are well below the porosities generated by the established TWA process (porosity 11.6%; target value < 16%, as measured in previous internal unpublished studies).

The pore size distribution plays an important role in the coating of cylinder running surfaces. Both the pores after the honing process and the honing marks provide space for oil retention. These must be matched to the tribological system. The influence on the pore size distribution and their size is therefore relevant for the quality of the cylinder coating (Ref 11). Furthermore, the pore size distribution was measured for < 10, 10-20 and > 20 μm^2 (see Fig. 10). In this study, 69.7% of the pores in coating 316L were smaller than 10 μm^2. For coating M3/2, 81.0% of the pores were smaller than 10 μm^2, while for coating E, 83.3% of all pores were smaller than 10 μm^2. In the range of > 20 μm^2, the result was inverted: 20.3% of all pores were larger than 20 μm^2 for coating 316L, while the values for

**Table 2** Chemical composition determined by EDX analysis

Element	Chemical composition, %					
	316L powder	316L coating	M3/2 powder	M3/2 coating	E powder	E coating
Iron (Fe)	61.0	62.2	72.1	75.4	93.0	90.2
Chromium (Cr)	18.7	17.3	4.0	4.2	0.6	0.8
Nickel (Ni)	12.7	12.2	…	…	4.3	4.1
Tungsten (W)	…	…	6.0	3.9	…	…
Vanadium (V)	…	…	5.6	4.2	…	…
Molybdenum (Mo)	2.9	3.1	6.6	5.7	…	…
Carbon (C)	2.5	1.8	4.8	3.3	1.6	1.5
Manganese (Mn)	1.4	1.7	0.3	0.7	…	…
Oxygen (O)	0.4	1.3	0.6	2.6	0.4	3.3
Silicon (Si)	0.4	0.4	…	…	0.1	0.1
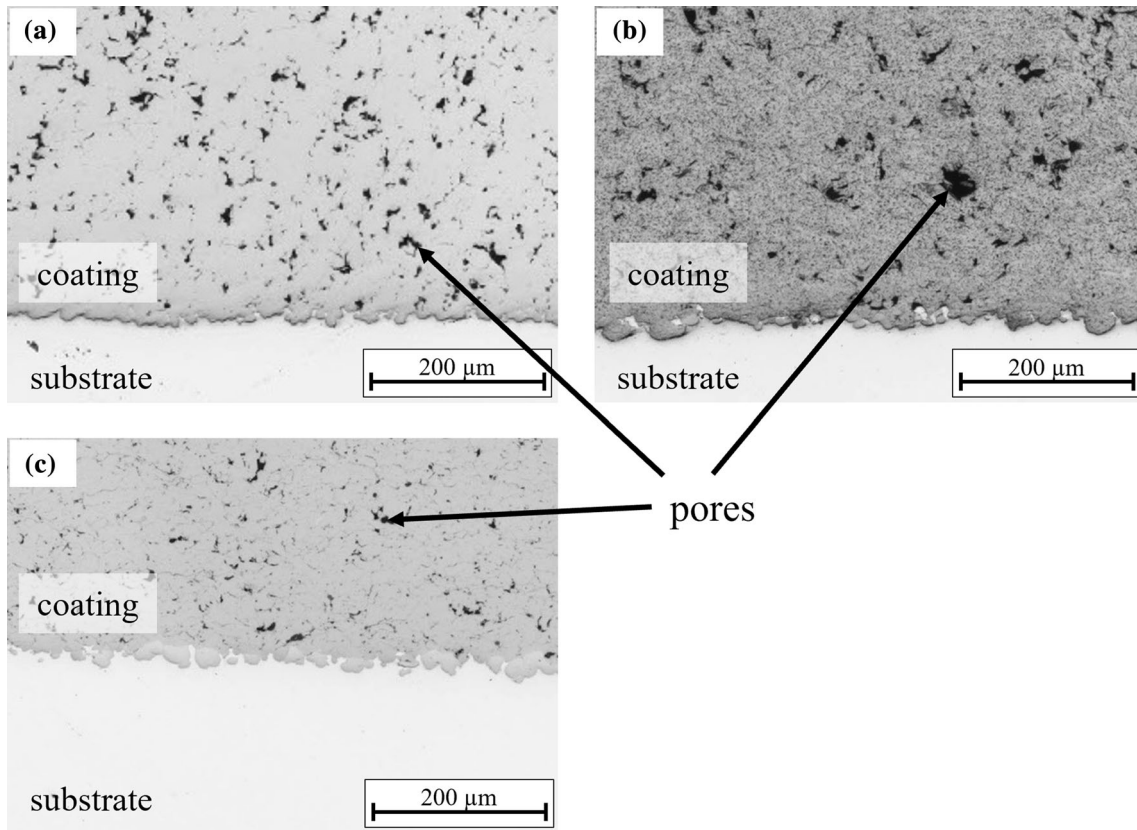
Fig. 8 Microscopic cross sections of the coatings with powders used in the experiments: (a) 316L; (b) M3/2; (c) E
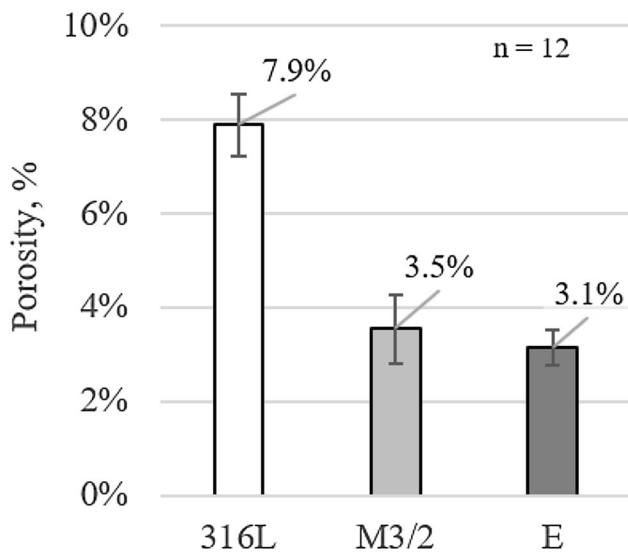
Fig. 9 Porosity for the final parameter set. Powder variants used: 316L, M3/2 and E. Number of measurements = n. Error bars represent the standard deviation (1 sigma)
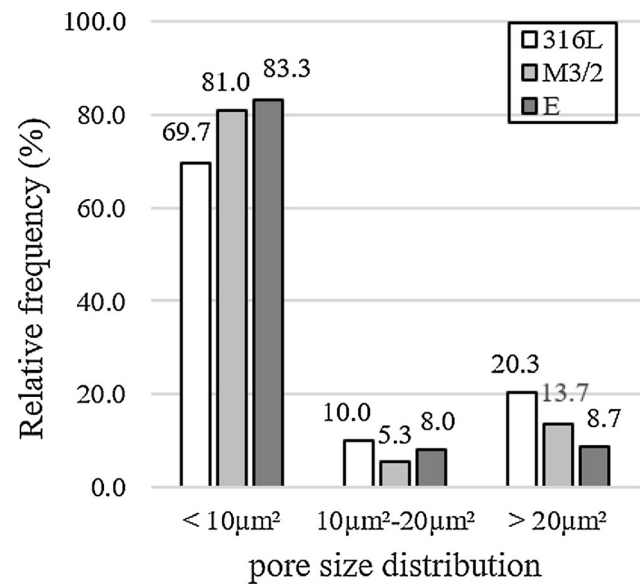
Fig. 10 Pore size distribution within the different coatings: < 10 μm^2, 10-20 μm^2 and > 20 μm^2

coating M3/2 and coating E were 13.7 and 8.7%, respectively. The results from this work confirm the observations from previous investigations. It is known from the literature that the pore size distribution decreases when the gas temperature increases, the gas pressure increases, the particle speed increases, or the particle size decreases (Ref 37-40).

Table 3 Hardness of the feedstock powder and CGS coating (12 measurements per variant)

	Powder hardness (HV0.025)	Coating hardness (HV0.025)	Ratio, %
316L	215 ± 19	376 ± 24	175
M3/2	219 ± 16	359 ± 35	164
E	153 ± 9	305 ± 16	199
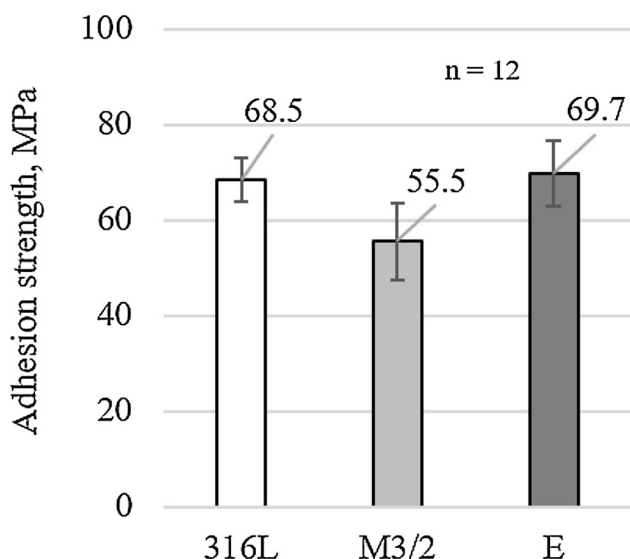
Fig. 11 Adhesion strength for the final parameter set. Powder variants used: 316L, M3/2 and E. Number of measurements = n. Error bars represent the standard deviation (1 sigma)

At the same cross sections, the results of the hardness measurements are illustrated in Table 3 for the different feedstock powders and their CGS coatings. The hardness of the material increased from the powder form to the coating form for all three variants tested. One of the reasons for this is that the high particle velocity in the CGS process severely plastically deforms the particles, resulting in strain hardening (Ref 36-41). For 316L and M3/2, the hardness ratios of the powder to coating are 175 and 164%, respectively. On the other hand, the hardness ratio of variant E is 199%, which is due to the significantly higher particle velocity obtained in the CGS process. However, the coating hardness corresponding to the established TWA process is significantly higher (865.5 HV0.025), which is attributed to the oxidation of the feedstock during the coating process.

Adhesion Strength

In contrast to conventional thermal spraying technologies, for CGS coating, preparation of the sample surface is not required. After coating, the samples were exposed to the pull-off test described above. Figure 11 shows the results of the adhesion strength measurements. In these tests, three liners were measured for each powder variant. For each

liner, four measurements were conducted along the coated surface (see Fig. 2). The positioning of the removal stamp had no influence on the adhesion strength. The coatings of the powder variants 316L and E displayed adhesion strengths of 68.5 and 69.7 MPa, respectively, which are close to the maximal value attained by the utilized FM 1000 glue (maximum adhesion strength of approximately 70 MPa). The adhesion strength of these two coatings was likely to be higher than the maximal preset threshold of 70 MPa, which was set by the glue properties. In contrast, powder M3/2 had a lower adhesion strength (55.5 MPa). The adhesion strength requirement of a thermal spray cylinder coating is approximately 30 MPa (Ref 11). Since all three coating variants examined in this article have strengths greater than 30 MPa, no breakout of the coating was expected in the subsequent honing process.

Figure 12(a) shows the test point of the liner with an M3/2 coating after the pull-off test. The failure of the M3/2 coating in this illustration was cohesive. For this reason, the maximum adhesion strength (70 MPa) of the glue was not achieved when using coating M3/2 (see Fig. 11). In contrast, Fig. 12(b) represents the test point of the liner with a 316L coating after the pull-off test. Most of the glue was still adhered to the coating; the connection in the glue failed. For this reason, the maximum adhesion strength between the glue and substrate was reached with the coating 316L and E examples. Figure 13(b) and 15(a) and shows the cross sections of the two samples from Fig. 12.

Figure 13(a) shows that the layer thickness of the CGS coating inside the former test stamp area was significantly lower than that outside the test point area, which is explained by the failure of the coating. Figure 13(b) shows that the coating of the 316L powder maintained its full thickness within the test stamp area. In conclusion, the adhesion strengths of coatings 316L and E exceeded the adhesion strength of the glue used and are therefore thought to be higher than 70 MPa. In contrast, lower adhesion strengths are generated by TWA processes (38.7 MPa, measured in earlier internal unpublished studies).

Honing and Wear Resistance

To obtain the appropriate roughness and shape of the coated liners, postprocessing on a honing machine was necessary. The cutting stones of the honing machine had

Fig. 12 Overview of the measuring points on the liners after the pull-off tests: (a) coating M3/2; (b) coating 316L
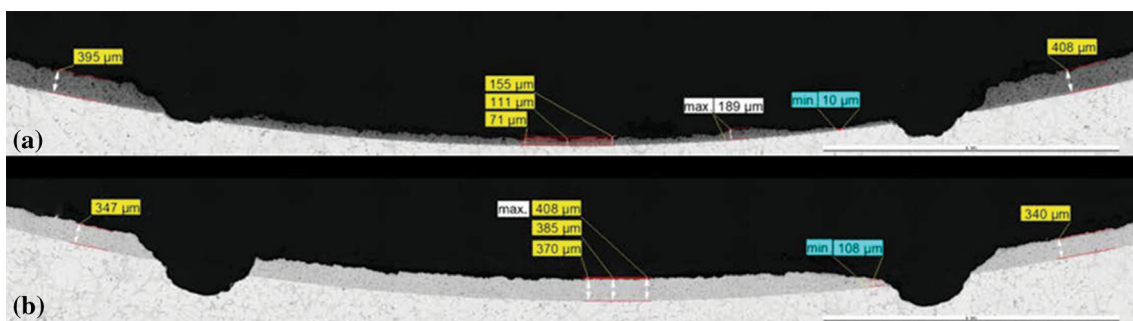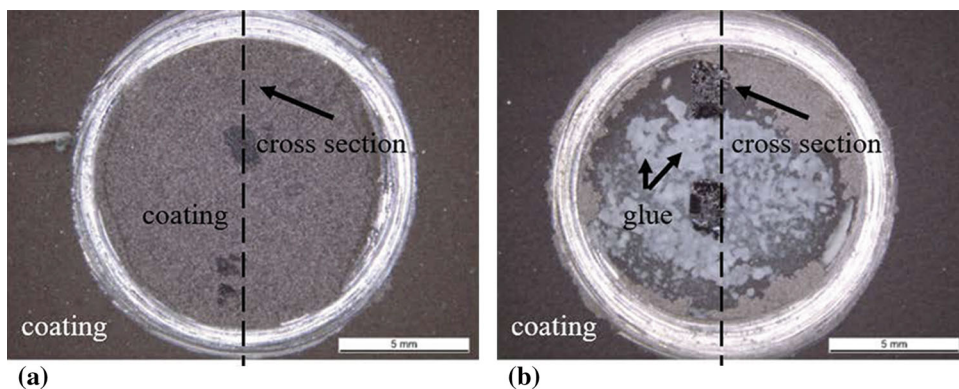
Fig. 13 Cross sections of the different types of connection failure: (a) cohesion: coating M3/2; (b) adhesion: coating 316L and coating E

the hardness of the CGS coating. Replica images of the cylinder surface were then taken by a conventional technique and used to examine surface quality after the honing process. In these images, no breakouts from the layer were detected in all coating variants, which usually complicates postprocessing after CGS coating (Ref 23).

Figure 14 shows the mean roughness depth (Rz) after the honing process. Coating M3/2 had the highest mean roughness depth at 2.67 µm. Coating 316L and coating E showed lower values of 1.85 and 1.44 µm, respectively. Therefore, the mean roughness after honing ultimately depended on the particle size distribution of the powder (Fig. 15). In fact, the higher the particle size distribution is, the higher the mean roughness depth at the end of the process (powder M3/2 > powder 316L > powder E). Notably, this correlation does not necessarily have to be correct for powders M3/2 and E, since the DE is not high (see Fig. 7). With a lower DE, there is no certainty that all particle sizes within a powder will be deposited during the coating process.

In Fig. 15, the coefficient R^2 shows a linear relationship to the mean roughness depth (Rz) across all three particle sizes (d10, d50 and d90). The following relationship was obtained: $R^2_{Rz/d10} < R^2_{Rz/d50} < R^2_{Rz/d90}$.

This means that with d-values, especially the d90-value, which typically includes more particles than the other
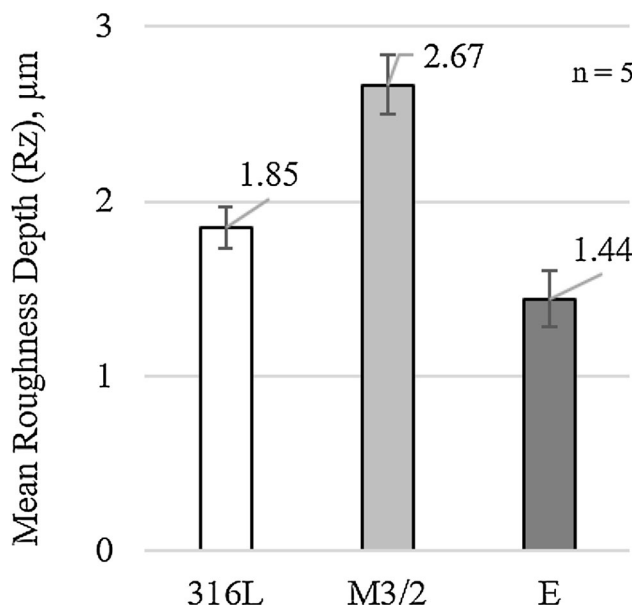
Fig. 14 Mean roughness depth (Rz) after the honing process for coating variants 316L, M3/2 and E. The number of measurements = n. Error bars represent the standard deviation (1 sigma)

d-values, one can predict the mean roughness depth (Rz) after honing.

Since small particle sizes in the CGS process are used, the mean surface roughness after honing was significantly finer in this research compared to that of the approved
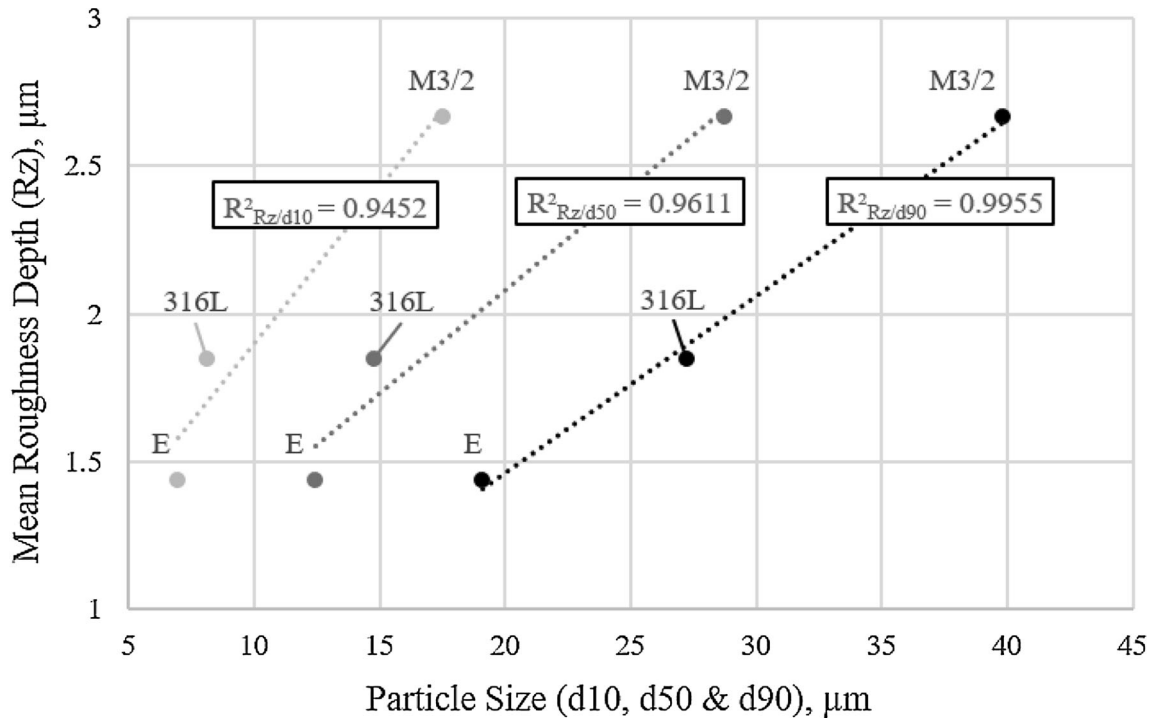
Fig. 15 Correlation between mean roughness depth (Rz) after honing and the particle size distribution before coating
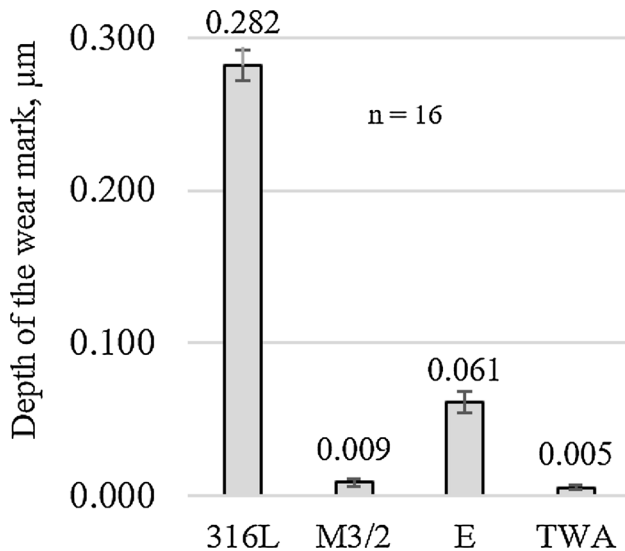
Fig. 16 Depth of the wear mark after ball-on-disk test for CGS coating variants. The BMW series coating (TWA) for cylinder running surfaces is considered as a reference. Number of measurements = n. Error bars represent the standard deviation (1 sigma)

TWA process ($Rz = 9.2\mu m$, as measured in previous internal unpublished studies).

The requirement for a suitable cylinder surface coating is a high wear resistance. Figure 16 shows the results of the ball-on-disk test. To compare the wear resistance values of the CGS samples, Fig. 16 also illustrates a reference

measurement of an established BMW series coating technology (TWA) for cylinder surfaces.

Although the three coatings are similar in hardness, the wear differs significantly. The coating of the 316L powder showed the deepest wear depth of 0.282 mm after the experiment. In contrast, coating E had a lower wear mark depth (0.061 mm), while the shallowest wear depth was observed in the coating of powder M3/2 (0.009 mm). The difference in wear resistance between the 316L and E coatings can be due to oxidation of the coating. The low wear of the M3/2 coating is due to the carbides (MC and M6C) in the feedstock. This is in accordance with prior investigations, which have shown that hard carbides significantly increase the wear resistance of materials (Ref 27, 28). In this study, the coating of powder M3/2 supported these observations. In comparison to the usually attained wear resistances of TWA coatings (material number: 1.0616; wear depth: 0.005 mm), the wear depth of coating M3/2 was only slightly deeper.

Conclusion

This study shows that liners with an inner diameter of 82 mm can be coated with CGS technology using a 90° angle head and a short nozzle. Three different alloy steel powder variants (316L, M3/2 and E) with different chemical compositions, particle sizes and morphologies were

used for the experiments. In conclusion, this research provided the following results:

- The higher the process parameters are, the better the CGS coating properties. In this study, the maximum parameter set of the system was 60 bar and 1000 °C.
- An increase in the hardness of the feedstock during the coating process was facilitated through strain hardening and was observed for all powder variants.
- The maximum adhesion strength (70 MPa) of FM 1000 glue was achieved with coating 316L and coating E. Coating M3/2 cohesively failed during the removal measurements at an adhesion strength of 55.5 MPa. The adhesion strengths of CGS coatings were significantly higher than the adhesion values achievable with the comparable TWA process.
- The mean surface roughness after honing correlated with the particle size in all three powder variants, with a strong linear relationship of $R^2 = 0.9955$.
- Wear-resistance tests revealed a significant difference among the three coatings. Powder M3/2 with carbides was particularly suitable for further investigation because the wear resistance was equivalent to the values acquired with the TWA coating process.

References

1. N. Dudareva, R.D. Enikeev and V. Ivanov, Thermal Protection of Internal Combustion Engines Pistons, *Procedia Eng.*, 2017, **206**, p 1382-1387.
2. F. Cuenot, CO2 Emissions from New Cars and Vehicle Weight in Europe; How the EU Regulation Could Have Been Avoided and How to Reach it?, *Energy Policy*, 2009, **37**(10), p 3832-3842.
3. M. Hahn and A. Fischer, Characterization of Thermal Spray Coatings for Cylinder Running Surfaces of Diesel Engines, *J. Therm. Spray Technol.*, 2010, **19**(5), p 866-872.
4. K. Kohashi, Y. Kimura, M. Murakami and Y. Drouvin, Analysis of Piston Friction in Internal Combustion Engine, *SAE Int. J. Fuels Lubr.*, 2013, **6**(3), p 589-593.
5. R.P. Vishwakarma and K.M. Rafi, Internal Combustion Engine, *Glob. Sci-Te.*, 2016, **8**(2), p 109.
6. D.E. Richardson, Review of Power Cylinder Friction for Diesel Engines, *J. Eng. Gas Turbines Power*, 2000, **122**(4), p 506-519.
7. G. Barbezat, Advanced Thermal Spray Technology and Coating for Lightweight Engine Blocks for the Automotive Industry, *Surf. Coat. Technol.*, 2005, **200**(5-6), p 1990-1993.
8. B. Gérard, Application of Thermal Spraying in the Automobile Industry, *Surf. Coat. Technol.*, 2006, **201**(5), p 2028-2031.
9. W. Tillmann and M. Abdulgader, Wire Composition: Its Effect on Metal Disintegration and Particle Formation in Twin-Wire Arc-Spraying Process, *J. Therm. Spray Technol.*, 2013, **22**(2-3), p 352-362.
10. J. Lee, J. Kim, C. Lee, Effects of carbon contents and gas type on hardness and wear resistance of ferrous coating fabricated by twin wire arc spray process, 235-238 (2017)
11. K. Bobzin, F. Ernst, K. Richardt, T. Schlaefer, C. Verpoort and G. Flores, Thermal spraying of cylinder bores with the Plasma Transferred Wire Arc process, *Surf. Coat. Technol.*, 2008, **202**(18), p 4438-4443.
12. R. Paredes, S.C. Amico and A. d'Oliveira, The Effect of Roughness and Pre-Heating of the Substrate on the Morphology of Aluminium Coatings Deposited by Thermal Spraying, *Surf. Coat. Technol.*, 2006, **200**(9), p 3049-3055.
13. A. Papyrin, V. Kosarev, S. Klinkov, A. Alkimov and V. Fomin, *Cold spray technology*, Elsevier, Amsterdam, 2007.
14. H. Assadi, F. Gärtner, T. Stoltenhoff and H. Kreye, Bonding Mechanism in Cold Gas Spraying, *Acta Mater.*, 2003, **51**(15), p 4379-4394.
15. T. Hussain, D.G. McCartney, P.H. Shipway and D. Zhang, Bonding Mechanisms in Cold Spraying: The Contributions of Metallurgical and Mechanical Components, *J. Therm. Spray Technol.*, 2009, **18**(3), p 364-379.
16. H. Assadi, T. Schmidt, H. Richter, J.-O. Kliemann, K. Binder, F. Gärtner, T. Klassen and H. Kreye, On Parameter Selection in Cold Spraying, *J. Therm. Spray Technol.*, 2011, **20**(6), p 1161-1176.
17. R. Maestracci, A. Sova, M. Jeandin, J.-M. Malhaire, I. Movchan, P. Bertrand and I. Smurov, Deposition of Composite Coatings by Cold Spray Using Stainless Steel 316L, Copper and Tribaloy T-700 Powder Mixtures, *Surf. Coat. Technol.*, 2016, **287**(4), p 1-8.
18. S. Dosta, G. Bolelli, A. Candeli, L. Lusvarghi, I. Garcia Cano and J. Maria Guilemany, Plastic Deformation Phenomena During Cold Spray Impact of WC-Co Particles onto Metal Substrates, *Acta Materialia*, 2017, **124**, p 173-181.
19. V.K. Champagne, Repair of magnesium components by cold spray techniques, *The Cold Spray Materials Deposition Process*. Woodhead Publishing, 2007, p 327-352
20. V.K. Champagne, P.F. Leyman and D.J. Helfritch, *Magnesium Repair by Cold Spray*, Army Research Laboratory, 2008, p 1-34
21. A. Papyrin, Cold Spray Technology, *Adv. Mater. Process.*, 2001, **9**(159), p 49.
22. J. Vlcek, L. Gimeno, H. Huber and E. Lugscheider, A Systematic Approach to Material Eligibility for the Cold-Spray Process, *J. Therm. Spray Technol.*, 2005, **14**(1), p 125-133.
23. L. Aubanel, L. Lefeivre, F. Delloro, M. Jeandin, E. Sura, Cold Spray Coatings for Automotive Cylinder Block Application, ITSC 2019 - Proceedings of the International Thermal Spray Conference, 433-440 2019
24. P. Richter, L. Holzgassner, J. Kondas and R. Singh, *Advancements in Cold Spray - Equipment, Materials, and Selected Applications, 11th Colloquim High Velocity Oxy-Fuel Flame Spraying*, Erding, Germany, 2018.
25. M. Villa, S. Dosta and J.M. Guilemany, Optimization of 316L Stainless Steel Coatings on Light Alloys Using COLD Gas Spray, *Surf. Coat. Technol.*, 2013, **235**, p 220-225.
26. R.F. Vaz, A. Silvello, J. Sanchez, V. Albaladejo and I. García Cano, The Influence of the Powder Characteristics on 316L Stainless Steel Coatings Sprayed by Cold Gas Spray, *Coatings*, 2021, **11**(2), p 168.
27. K. Amini, A. Akhbarizadeh and S. Javadpour, Effect of Deep Cryogenic Treatment on the Formation of Nano-Sized Carbides and the Wear Behavior of D2 Tool Steel, *Int. J. Miner., Metall., Mater.*, 2012, **19**(9), p 795-799.
28. K. van Acker, D. Vanhoyweghen, R. Persoons and J. Vangrunderbeek, Influence of Tungsten Carbide Particle Size and Distribution on the Wear Resistance of Laser Clad WC/Ni Coatings, *Wear*, 2005, **258**(1-4), p 194-202.

29. M.R. Rokni, C.A. Widener and G.A. Crawford, Microstructural evolution of 7075 Al gas atomized powder and high-pressure cold sprayed deposition, *Surf. Coat. Technol.*, 2014, **251**, p 254-263.

30. J. Wu, H. Fang, S. Yoon, H. Kim and C. Lee, Measurement of Particle Velocity and Characterization of Deposition in Aluminum Alloy Kinetic Spraying Process, *Appl. Surf. Science*, 2005, **252**(5), p 1368-1377.

31. B. Jodoin, L. Ajdelsztajn, E. Sansoucy, A. Zúñiga, P. Richer and E.J. Lavernia, Effect of Particle Size, Morphology, and Hardness on Cold Gas Dynamic Sprayed Aluminum Alloy Coatings, *Surf. Coat. Technol.*, 2006, **201**(6), p 3422-3429.

32. V.K. Champagne, D.J. Helfritch, S.P.G. Dinavahi and P.F. Leyman, Theoretical and Experimental Particle Velocity in Cold Spray, *J. Therm. Spray Technol.*, 2011, **20**(3), p 425-431.

33. G. Mauer, R. Singh, K.-H. Rauwald, S. Schrüfer, S. Wilson and R. Vaßen, Diagnostics of Cold-Sprayed Particle Velocities Approaching Critical Deposition Conditions, *J. Therm. Spray Technol.*, 2017, **26**(7), p 1423-1433.

34. DIN EN ISO 14917 (2017) Thermisches Spritzen - Begriffe, Einteilung (Thermal spraying - Terminology, classification), (in German)

35. X.-J. Ning, J.-H. Jang and H.-J. Kim, The Effects of Powder Properties on In-Flight Particle Velocity and Deposition Process During Low Pressure Cold Spray Process, *Appl. Surf. Sci.*, 2007, **253**(18), p 7449-7455.

36. W. Wong, P. Vo, E. Irissou, A.N. Ryabinin, J.-G. Legoux and S. Yue, Effect of Particle Morphology and Size Distribution on Cold-Sprayed Pure Titanium Coatings, *J. Therm. Spray Technol.*, 2013, **22**(7), p 1140-1153.

37. W. Wong, E. Irissou, A.N. Ryabinin, J.-G. Legoux and S. Yue, Influence of Helium and Nitrogen Gases on the Properties of Cold Gas Dynamic Sprayed Pure Titanium Coatings, *J. Therm. Spray Technol.*, 2011, **20**(1-2), p 213-226.

38. P. Richer, M. Yandouzi, L. Beauvais and B. Jodoin, Oxidation Behaviour of CoNiCrAlY Bond Coats Produced by Plasma, HVOF and Cold Gas Dynamic Spraying, *Surf. Coat. Technol.*, 2010, **204**(24), p 3962-3974.

39. S.H. Zahiri, D. Fraser, S. Gulizia and M. Jahedi, Effect of Processing Conditions on Porosity Formation in Cold Gas Dynamic Spraying of Copper, *J. Therm. Spray Technol.*, 2006, **15**(3), p 422-430.

40. S.H. Zahiri, C.I. Antonio and M. Jahedi, Elimination of PORosity in Directly Fabricated Titanium via Cold Gas Dynamic Spraying, *J. Mater. Process. Technol.*, 2009, **209**(2), p 922-929.

41. T.H. van Steenkiste, J.R. Smith and R.E. Teets, Aluminum Coatings via Kinetic Spray with Relatively Large Powder Particles, *Surf. Coat. Technol.*, 2002, **154**(2-3), p 237-252.